Noname manuscript No.
(will be inserted by the editor)

Minimal surface configurations for axisymmetric microparticles

Kyung Ha · Joseph de Rutte · Dino Di Carlo · Andrea Bertozzi

Received: date / Accepted: date

Abstract An important area of microfluidics is the creation and manipulation of small droplets. This is commonly done using microchannels or electrowetting. Recently a new method is proposed to create templated droplets using cup-shaped microparticles. These particles are observed to hold nearly identical volumes of aqueous liquid when dispersed in an oil-water mixture. However a theory for this behavior is lacking. In this paper we present a mathematical model for such minimal surface configurations in the case of axisymmetry. We obtain a volume-energy graph by finding the minimal surface for various volumes and develop a theory regarding the exchange of fluid between multiple particles.

Keywords Minimal surfaces · Microfluidics · Surface tension · Volume constraint optimization · Droplets

Kyung Ha
Department of Mathematics, University of California, Los Angeles, CA 90095 USA
E-mail: kyungha@g.ucla.edu

Joseph de Rutte
Department of Bioengineering, University of California, Los Angeles, CA 90095 USA
E-mail: jderutte@ucla.edu

Dino Di Carlo
Department of Bioengineering, Mechanical and Aerospace Engineering , Los Angeles, CA 90095 USA
E-mail: dicarlo@ucla.edu

Andrea Bertozzi
Department of Mathematics, Mechanical and Aerospace Engineering , University of California, Los Angeles, CA 90095 USA
E-mail: bertozzi@math.ucla.edu

1 Introduction

The creation and manipulation of fixed sized miniature droplets is an important area of study in microfluidics, enabling highly sensitive biological and chemical assays. A benefit of such technology is that by compartmentalizing a larger volume into sub-components, individual cells or molecules can be analyzed more precisely. This is because the secretion of molecules from a cell, or the products of reactions of individual molecules, can quickly accumulate to high concentrations when confined in small volumes. Conventional technologies are focused on droplet formation and manipulation via flow in microchannels [1,2,3] or in electrowetting devices [4,5,6]. Another approach, recently developed, is the creation of tiny solid particles with complex geometries and hydrophilic parts that allow for the capture of uniform sized droplets simply by having favored conditions related to their surface energy [7,8] (Fig. 1). These microparticles can result in stable isolated volumes on the nanoliter or sub-nanoliter scale, when simply mixed. Molecules accumulating in these small volumes at high concentration can also bound to the solid phase of the particle, enabling analysis with standard equipment like flow cytometers. This can lead to "lab on a particle" technologies in which experiments can be done on thousands of individual cells, to study phenomena at the cellular level.

A theory behind this new technology is lacking though. We are interested in understanding two problems: (a) the optimal surface energy configuration for specific microparticle designs; and (b) the optimal energy configuration for a multi-particle system. We calculate the energy related to surface tensions only, since it is the dominant contributor at the microscale compared to other forces, for example buoyancy.

Finding a configuration that minimizes surface tension while maintaining a certain volume is a classical problem in geometry [10,11]. One especially well documented case is the problem of a liquid bridge between two axisymmetric surfaces. A common example of such surfaces are spheres [12,13,14] and planes. The planes are in various shapes that either expand to infinity [15,16,17, 18,19], are finite [20,21,22,23,24,25,26,27], or a mix of both conditions [28]. Results with more general shapes are well documented in [29].

In this paper we investigate minimal surface configurations for more complex axisymmetric solids (Fig. 2) for which there exists experimental data [9, 30]. In this case the ensuing minimization problem is reduced to a 1D problem and is relatively straightforward so rigorous results are derived. Moreover, such symmetry often corresponds to simplified manufacturing technologies for producing such particles in bulk. It is possible to achieve minimal surfaces without the axisymmetric assumption using 3D simulations as in [7]. However this is computationally expensive compared to 1D simulations. Once we obtain the minimal surface of a single particle we study how particles interact with each other by distributing a fixed volume of fluid. We solve this by distributing the fluid so that the total surface energy is minimized. Under this assumption we develop a theory for the minimal energy configuration of multi-particle systems for a given total volume. Simulations of such interactions help us understand

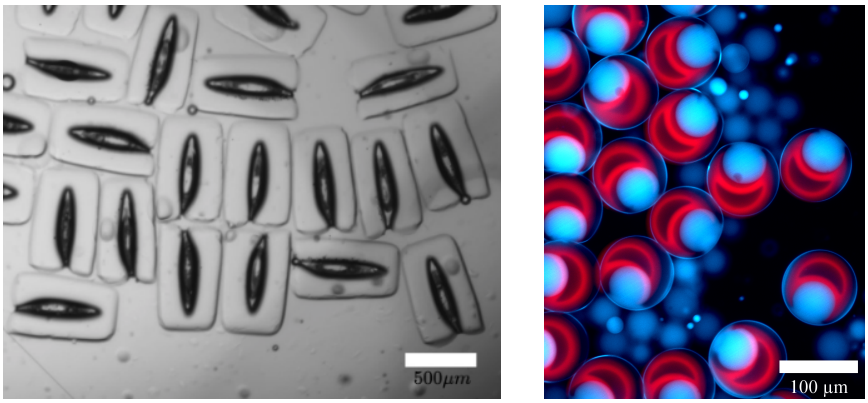

(a) (b)

Fig. 1: Experimental photos of "dropicles". In both images water is captured inside the the particles which are surrounded by oil. In (a) the particles are those in [7], which are not axisymmetric and have a fully 3D structure. The particles in (b) are those in [9] and are shaped as in Fig 2b. (b) is a false color image, with the particle colored red and water colored blue. The surrounding oil appears dark.

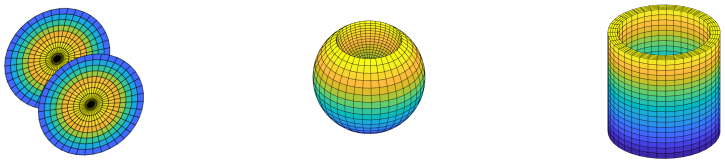

(a) Two parallel flat planes (b) Hollow sphere (c) Hollow Cylinder

Fig. 2: Shapes of axisymmtric microparticles. A cross-section of (b) and (c) are shown in Fig. 3b and 3c respectively.

the minimal energy configurations achieved through pairwise interactions and develop ideas for efficient particle design.

Our paper is organized as follows. In section 2, we explore three microparticle configurations of interest: planar surfaces, hollow spheres, and hollow cylinders (Fig. 2). We deduce the shape of the minimal surface and calculate the volume-energy graph for each particle. In section 3, we develop rigorous theory regarding the minimal configuration for a multi-particle system. We can predict the minimal energy distribution of multi-particle systems by observing properties of the volume-energy graph of a single dropicle. In section 4 and 5, we simulate the interaction between two and multiple particles respectively. The simulation verify the results in section 3 and also suggest guidelines for particle design. Through out the paper we follow the terminology in [7,8], by

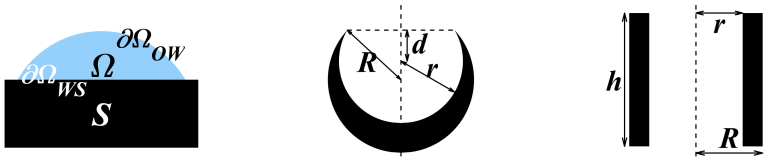

(a) (b) (c)

Fig. 3: Examples of water droplets adhering to solid surfaces. (a) is a droplet (blue) on an infinite flat surface (black). (b) and (c) are cross sections of a hollow sphere and a hollow cylinder, respectively, with the axis of symmetry shown as a dotted vertical line. The solids are colored in black. In (b), R and r are the radius of the outer and inner spheres respectively, and d is the offset between the tip of the particle and the center of the inner sphere. In the figure the parameters are $R = 1.18$, $r = 1$, and $d = 0.5$. In (c), h is the height and R and r are the inner and outer radius of the cylinder. In the figure the parameters are $R = 0.9$, $r = 0.7$ and $h = 3$.

denoting the target liquid as water, the surrounding liquid as oil. We denote the water-particle complex as a "dropicle".

2 Energy minimizing surfaces

In this section we focus on finding the minimal energy surface configuration for a given particle and volume. By repeating these calculations for different volumes, we draw a volume-energy graph (V-E graph) of a particle.

Denote the fixed solid region by S, the finite volume of water by Ω, the water-solid interface by $\partial\Omega_{WS}$ and the water-oil interface by $\partial\Omega_{WO}$. Note that $\partial\Omega = \partial\Omega_{WS} \cup \partial\Omega_{WO}$ (Fig. 3a). The interfacial tension energy of the dropicle is

$$\begin{aligned} E(\Omega) &= \sigma_{WO}|\partial\Omega_{WO}| + \sigma_{WS}|\partial\Omega_{WS}| + \sigma_{OS}(|\partial S| - |\partial\Omega_{WS}|) \\ &= \sigma_{WO}|\partial\Omega_{WO}| + (\sigma_{WS} - \sigma_{OS})|\partial\Omega_{WS}| + \sigma_{OS}|\partial S| \end{aligned} \tag{1}$$

where $|\partial S|$ is the surface area of the solid, $|\partial\Omega_{WO}|$ and $|\partial\Omega_{WS}|$ are the water-oil and water-solid surface areas of Ω respectively, σ_{WS}, σ_{WO} and σ_{OS} are surface tensions between water-solid, water-oil and oil-solid respectively. We assume the solid is hydrophilic and partial wetting happens, i.e.

$$\sigma_{WO} > \sigma_{OS} - \sigma_{WS} > 0. \tag{2}$$

Throughout this paper we use the surface tensions values $\sigma_{WO} = 1, \sigma_{WS} = 0.1$, and $\sigma_{OS} = 0.9$, unless stated otherwise. This choice is consistent with the use of hydrophilic materials for the solids in the experiments [7,9,8]. Qualitatively the results do not change much with modest variation in these parameters (c.f. Section 4.2). We note that the last term in (1) only depends on ∂S and is

independent of the water domain Ω so we ignore it as far as the minimal energy calculation is concerned. Also we note that the energy equation does not take any dynamics around the dropicle into account, and therefore our model is a static fluid model. We need to find an Ω that minimizes the energy (1) under the volume constraint $|\Omega| = V$. Since the ratio of surface energies determine the static problem the energy can be dimensionless. Throughout this paper we assume that for each dropicle Ω is an open bounded and connected domain.

Solving (1) is well documented in [29] chapter 2. The minimizing surface is a constant mean curvature surface, with a prescribed contact angle α satisfying,

$$cos\alpha = (\sigma_{OS} - \sigma_{WS})/\sigma_{WO} \tag{3}$$

called the Duprè-Young condition for smooth solid surfaces. For sharp surfaces (e.g. tips of Fig. 3b) we consider a range of contact angles rather than a single choice. The range depends on α and the angle of the sharp solid. A way to understand this is by smoothing the sharp surface locally and applying the condition in (3) to a specific point in the smoothed area.

The physical cases of interest here are all axisymmetric connected solids (Fig. 2b and 2c), with simply connected axisymmetric water domains. Under these assumptions the water-oil interface $\partial\Omega_{WO}$ of problem (1) is part of a sphere.

Theorem 1 *Assume the surface tensions satisfy the partial wetting condition (2) and the solid is axisymmetric and connected. Also assume that the water domain is bounded, simply connected and axisymmetric. Then the water-oil interface that minimizes (1) is part of a sphere.*

Proof. This theorem summarizes results discussed in detail in [29] chapter 2.4.4. □

The rest of this section uses this theoretical result to compute the energy-volume curves for the particle shapes of interest. We start with the classical case of two parallel planes, which are well-studied in the literature, to contrast with the hollow particle shapes that are less well-studied.

2.1 Two parallel planes

The parallel plane case is well-known [18]. In this case there are two types of geometries to consider for Ω: (a) a droplet that only touches one of the planes or (b) a bridge between the two planes.

Spherical cap: For the case where the water only comes into contact with one of the planes, since the surface is connected and axisymmteric, we obtain a spherical cap as the minimizer by applying Theorem 1. The size and shape of the sphere is decided from the volume constraint and the Duprè-Young condition.

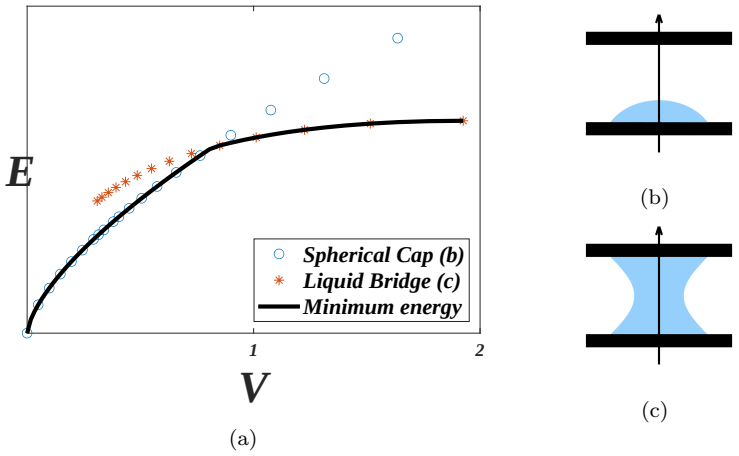

Fig. 4: Parallel plane dropicles. (a) is the V-E graph of parallel planes, while (b) and (c) are cross sections of the spherical cap and the liquid bridge through the axis of symmetry shown as a vertical arrow. The blue $\circ$ dots in (a) indicate the energy when the water is on one side and forms part of a sphere as in (b). The orange $*$ dots indicate the energy when the water forms a bridge connecting both sides as in (c). The unit volume is $(2a)^3$ where $2a$ is the distance between the parallel planes. The black solid line is the minimum of the two dotted lines and represents the V-E graph. The surface tensions are $\sigma_{WO} = 1$, $\sigma_{WS} = 0.1$, $\sigma_{OS} = 0.9$.

Liquid bridge : For the case when water connects both planes of distance $2a$, using calculus of variations, it is known [18] that an axisymmetric bridge forms with shape profile $f(x)$ between $-a$ and a satisfying,

$$\frac{f''}{(1+(f')^2)^{3/2}} - \frac{1}{f(1+(f')^2)^{1/2}} = 2H \tag{4}$$

where H is the Lagrange multiplier corresponding to the volume constraint, with Neumann boundary conditions

$$f'(-a) = \frac{\sigma}{\sqrt{1-\sigma^2}}, \quad f'(a) = -\frac{\sigma}{\sqrt{1-\sigma^2}} \tag{5}$$

where $\sigma = (\sigma_{WS} - \sigma_{OS})/\sigma_{WO}$ (Fig. 4c). The boundary conditions that arise are identical to those given by the Duprè-Young condition.

Fig. 4a shows the V-E graph of the spherical cap and the liquid bridge. The blue $\circ$ dotted line represents the V-E graph for the spherical cap attached to one of the planes, which was calculated by minimizing (1) under the volume constraint using basic calculus. The orange $*$ dotted lines represent the energy of the liquid bridge which is calculated by solving the ODE (4) and (5) numerically using the shooting method for a given range of H. The minimum

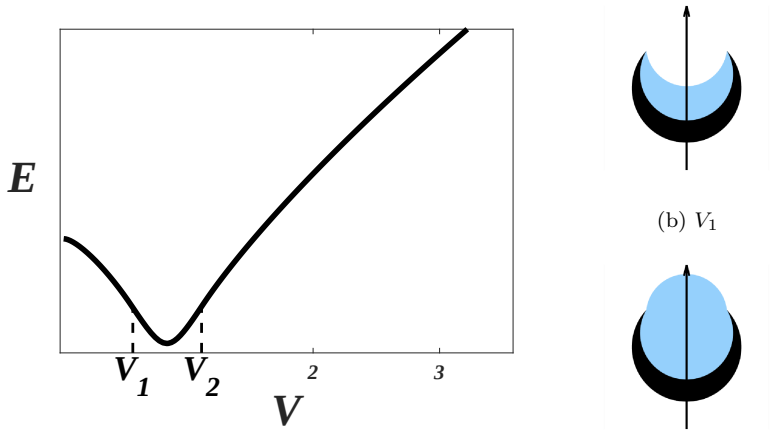

(a)

(b) V_1

(c) V_2

Fig. 5: Hollow sphere dropicle. (a) is the V-E graph of hollow sphere particle. The minimum is obtained when the water-oil interface is flat. (b) and (c) are cross sections of the dropicle through the axisymmetric axis. The volume contained in each image corresponds to the volumes V_1 and V_2 indicated on the graph. The parameters of the particle are those given in Fig. 3b. The unit volume is given as $V_{IS} = \frac{4}{3}\pi r^3$. The surface tensions are $\sigma_{WO} = 1$, $\sigma_{WS} = 0.1$, $\sigma_{OS} = 0.9$.

energy configuration for a given volume is the minimum of the two graphs, shown as the black solid line. This indicates that there is a transition from a spherical cap to a liquid bridge as we increase the volume.

2.2 Hollow sphere

Next we consider a particle shaped as in Fig. 2b, a larger sphere with a smaller inner sphere carved out to form an exposed cavity, which we call the hollow sphere. The parameters related to such a shape are given in Fig. 3b. We assume that the water-oil surface is axisymmetric with respect to the common axis of the two spheres (Fig. 5). By Theorem 1 the shape of the minimal water-oil surface is itself a spherical cap with a curvature that can differ from those of the particle surfaces. To precisely compute the V-E graph we follow the procedure as outlined below.

1. For a given water volume and circular triple junction (contact line), there exists one spherical surface. We compute the surface energy of the entire system for this chosen contact line.
2. Fix the volume and find the contact line which minimizes the energy of the system.

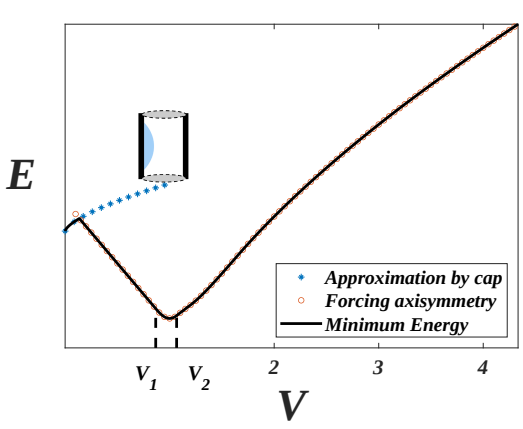

(a)

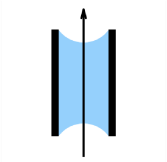

(b) V_1

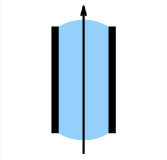

(c) V_2

Fig. 6: Hollow cylinder dropicle. (a) is the V-E graph of hollow cylinder particle. The blue $*$ represents an approximation of the non-axisymmetric surface by a surface of a cap (Fig. 4). The red $\circ$ represents the V-E graph when axisymmetry is forced. The black solid line is the minimum of these two cases which is close to the actual V-E graph. The minimum of the black line is obtained when the top and bottom water-oil interfaces are flat. (b) and (c) are cross sections of the dropicle through the axisymmetric axis. The water volume corresponds to the volumes V_1 and V_2 indicated on the graph. The parameters of the particle are given in Fig. 3c. The unit volume is given as the volume of the inner cylinder $V_{IC} = \pi r^2 h$. The surface tensions are $\sigma_{WO} = 1$, $\sigma_{WS} = 0.1$, $\sigma_{OS} = 0.9$.

3. Repeat the calculation for different volumes.

Fig. 5a shows the V-E graph of a hollow sphere particle with cross section shown in Fig. 3b. For small volumes of water, we see a decrease in energy as the volume increases, until the water volume is large enough so that it reaches the outer edge of the hollow sphere and forms a flat surface. Two special volumes of interest are V_1, the smallest volume for which the water droplet reaches the edge of the hollow sphere, and V_2, the largest such volume. Once the water volume exceeds V_2 the minimal surface wets the outside sphere. When the contact line is away from the sharp tip, the Duprè-Young condition holds for the minimal surface. However for the sharp corner the minimizing surface does not necessarily satisfy the condition.

2.3 Hollow cylinder

The particle we consider in this section is an empty cylinder with a finite wall width (Fig. 2c), which we call a hollow cylinder. The shape parameters are given in Fig. 3c. Again we assume that the water-oil surface is axisymmetric about the axis of the cylinder. By Theorem 1, the shape of the water-oil surface is part of a sphere. The V-E graph is calculated by a similar method as in 2.2. The difference is that the water-oil interface is comprised of two disjoint surfaces, top and bottom, that need to be determined. We determine the minimal energy configuration by calculating the energy of different combinations of top and bottom interfaces that contain the given volume. The results are plotted in Fig. 6a as red $\circ$. Similar to the hollow sphere, V_1 and V_2 denote the smallest and largest volumes for which the contact line of the droplet are edges of the hollow cylinder. When the contact line is away from the edges, again the Duprè-Young condition holds for the minimal surface, but not necessarily for the sharp corners. One should note that for small enough volumes the water domain that minimizes (1) is not axisymmetric. For such small volumes (as $V \to 0$) the water domain is similar to a spherical drop inside one side of the cylinder. For simplicity, we approximate this as a spherical cap on a flat plane, which we use for the minimal energy configuration for very small water drops inside a cylinder (blue $*$ in Fig. 6a). We do not focus on this detail though, because it is outside the range of interest for interacting dropicles. For this reason we need not compute it precisely and ignore this approximation for future simulations. The black solid line denotes the lowest energy configuration, of the red and blue graph. A phase change from axisymmetric to non-axisymmetric happens near the volume where the two intersect, as in the flat plane case (Fig. 4).

3 Rigorous theory of minimizing surface

In this section we answer how the V-E graphs can be used to analyze the interactive behavior between dropicles. We develop a theory for the minimal energy water distribution among multiple dropicles. First we consider two identical particles and a fixed total volume of water. The first derivative of the graph is key in understanding how to split the water between the particles to achieve energy minimum. Extending this idea we prove a theorem for systems with more than two particles. Throughout this paper we assume each dropicle contains only one particle, i.e. no two particles are connected by the same water droplet. In real physical systems, sometimes one observes coalescence of these dropicles. However this is beyond the scope of our current analysis.

3.1 Droplet splitting between two particles

For a particle along with its V-E graph, $E(V)$, we address the question of the optimal water distribution between two identical particles, given a fixed

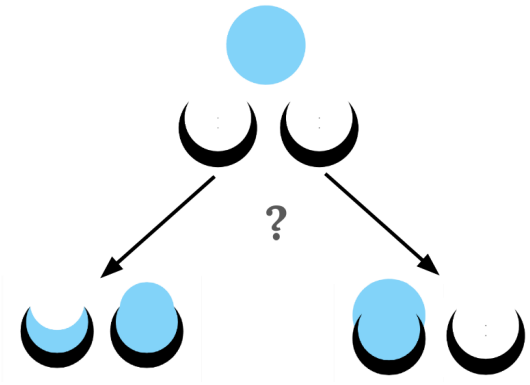

Fig. 7: What is the optimal way to split a volume of water between two particles?

total water volume V_T. Does the water droplet split into two smaller drops or remain intact (Fig. 7)? We formulate this as an optimization problem

$$\overline{V} = \underset{0 \leq V \leq V_T}{\arg\min} \{E(V) + E(V_T - V)\}. \tag{6}$$

This optimization problem minimizes the sum of the static energy function $E(V)$. For this paper we only consider functions $E(V)$ that are continuously differentiable.

By the symmetry of the problem we get two values of $\overline{V}$ that represent identical situations. We denote the smaller volume as V_S and the larger one as V_L. Without lost of generality finding solutions of $\overline{V}$ is identical to finding

$$V_S = \underset{0 \leq V \leq V_T/2}{\arg\min} \{E(V) + E(V_T - V)\}. \tag{7}$$

Since the domain is compact, there exists a minimizer either on the boundary ($V_S = 0$ and $V_S = V_T/2$) or when the first derivative is 0,

$$E'(V_S) = E'(V_T - V_S). \tag{8}$$

We need to know how V_S changes with respect to the total volume V_T.

3.1.1 Convex and Concave V-E graphs

For convex and concave $E(V)$, V_S is trivial.

Theorem 2 *Assume $E(V) \in \boldsymbol{C}^1[0, \infty)$. If $E(V)$ is a convex function, $V_S = V_T/2$. If $E(V)$ is a concave function, $V_S = 0$. If $E(V)$ is strictly convex or strictly concave, the minimizer is unique.*

Proof. If $E(V)$ for $0 \leq V \leq V_T$ is a convex function the total energy function $E(V) + E(V_T - V)$ is also a convex function. The minimum of the convex function is obtained where the first derivative is 0. This is satisfied for $V_S = V_T/2$. If $E(V)$ is strictly convex this minimizer is unique.

If E is a concave function, by using concavity twice we obtain

$$E(0) + E(V_T) \leq E(V) + E(V_T - V), \tag{9}$$

for all $0 \leq V \leq V_T$, hence $V_S = 0$. If $E(V)$ is strictly concave the inequality is strict. □

Classical example A simple example of the concave case is an isolated water droplet in the absence of a solid particle. Since the minimal surface of a water drop in oil is a sphere, the energy graph obeys $E(V) = \sigma_{WO}(6\sqrt{\pi}V)^{2/3}$, so the graph is strictly concave. Consequently any two spherical drops have surface area greater than that of a single sphere with the combined volumes.

3.1.2 General V-E graphs

For hollow sphere and hollow cylinder particles certain properties of $E(V)$ lead to guaranteed bounds on the size of V_S.

Theorem 3 *Consider two particles with the same V-E graph $E(V)$. Suppose $E(V) \in \boldsymbol{C}^1[0,\infty)$ has the following properties.*

1. *For some $0 < V_1 < V_2$, $E'(V)$ decreases for $0 \leq V \leq V_1$, strictly increases for $V_1 \leq V \leq V_2$ and again strictly decreases for $V_2 \leq V$.*
2. $\lim_{V\to\infty} E'(V) = 0$.
3. $\int_0^{V_2} E'(U)dU = E(V_2) - E(0) \leq 0$.

For water of total volume V_T the following are true for V_S defined in (7),

1. *If $0 \leq V_T \leq V_1$, then $V_S = 0$ i.e. the minimal surface energy configuration is one particle containing all water.*
2. *There exist $V_b \geq V_2$, so that if $2V_b \leq V_T$, then $V_1 \leq V_S \leq V_2$ i.e. there exists a particle containing a water volume in the range $[V_1, V_2]$.*

The second result of the above theorem is important because it results in fairly uniform size volumes (between V_1 and V_2) associated with a particle. With many particles a similar result holds in which all but one particle have a volume of water between these two bounds (cf. Fig. 14). A particle with a V-E graph that yields V_1 close to V_2 should trap a droplet with a specific volume between the two and this is a design feature of the system.

Proof. Fig. 8a is an example of a function that satisfies the conditions of the theorem. The first conclusion follows from the fact that since $E'(V)$ is decreasing for $0 \leq V \leq V_1$, therefore $E(V)$ is concave in this range. We conclude from Theorem 2 that $V_S = 0$.

The second conclusion is proved as follows. Recall that V_S, if it is not 0, should satisfy equation (8). If $V_T \geq 2V_2$ this leads to $E'(V_T - V) > 0$. Therefore in this case the first condition in the theorem restricts us as having at most four possible candidates of V_S, which are $V = 0$, $0 < V_\alpha < V_1$, $V_1 \leq V_\beta \leq V_2$ and $V = V_T/2$. We show that the energy of V_β is smaller than the rest when V_T is greater than $2V_b$ for some V_b.

(a) Compare $V = 0$ and $V_1 \leq V_\beta \leq V_2$:
We show that

$$E(V_T) + E(0) - E(V_T - V_\beta) - E(V_\beta) \geq 0$$

for any $V_1 \leq V_\beta \leq V_2$ that satisfies (8). If we write each component of the left hand side as an integral of E', it is identical to

$$\int_{V_T - V_\beta}^{V_T} E'(U)dU - \int_0^{V_\beta} E'(U)dU$$

which is greater or equal than

$$-\int_0^{V_\beta} E'(U)dU.$$

The inequality comes from the fact that $E'(U) > 0$ for $U > V_2$. Since $E'(V_T - V_\beta) > 0$ and V_β satisfies equation (8), $E'(V_\beta) > 0$. This with the fact that $E'(V)$ increases in the domain $V_\beta < U < V_2$, from the first condition of the theorem, indicates that for such U, $E'(U) > 0$. Therefore

$$-\int_0^{V_\beta} E'(U)dU \geq -\int_0^{V_2} E'(U)dU \geq 0 \tag{10}$$

by the third condition of the theorem.

(b) Compare $0 < V_\alpha < V_1$ and $V_1 \leq V_\beta \leq V_2$:
Following the steps in the previous comparison it is sufficient to show

$$-\int_{V_\alpha}^{V_\beta} E'(U)dU \geq 0.$$

From the fact that V_α satisfies equation (8) and that $E'(V)$ decreases for $0 < U < V_\alpha$, gives $E'(U) > 0$ for such U. Therefore combining this with (10), we deduce

$$-\int_{V_\alpha}^{V_\beta} E'(U)dU \geq -\int_0^{V_2} E'(U)dU \geq 0.$$

(c) Compare $V = V_T/2$ and $V_1 \leq V_\beta \leq V_2$:
Again we show

$$-\int_{V_T/2}^{V_T - V_\beta} E'(U)dU + \int_{V_\beta}^{V_T/2} E'(U)dU \geq 0.$$

Note that

$$-\int_{V_T/2}^{V_T-V_\beta} E'(U)dU \geq -\int_{V_T/2}^{V_T-V_\beta} E'(V_T/2)dU = -\int_{V_\beta}^{V_T/2} E'(V_T/2)dU$$

therefore, showing

$$\int_{V_\beta}^{V_T/2} E'(U) - E'(V_T/2)dU \geq 0$$

is sufficient. Now we pick V_b. Since there exists a W_0 between V_1 and V_2 that $E'(W_0) = 0$ (W_0 is the minimum of $E(V)$ graph). This comes from the first and third condition of $E(V)$. Also since E' strictly increases before V_2 and strictly decreases after V_2 converging to 0, we have a one to one correspondence between V and W which satisfies $E'(V) = E'(W)$ lying in the domain $W_0 \leq W \leq V_2$ and $V_2 \leq V$. We pick a V_b so that the W_b corresponding to V_b satisfies

$$\int_{W_0}^{W_b} E'(V_b)dU \leq \int_{W_b}^{V_b} E'(U) - E'(V_b)dU \tag{11}$$

is satisfied. Such V_b exists because the left hand side goes to 0 as V_b goes to infinity, while the right hand side increases from a nonzero value (cf. Fig. 8a).
Then for $V_T \geq 2V_b$

$$\begin{aligned}
&\int_{V_\beta}^{V_T/2} E'(U) - E'(V_T/2)dU \\
&\geq \int_{V_\beta}^{W_b} E'(U) - E'(V_b)dU + \int_{W_b}^{V_T/2} E'(U) - E'(V_T/2)dU &(12)\\
&\geq \int_{W_0}^{W_b} E'(U) - E'(V_b)dU + \int_{W_b}^{V_b} E'(U) - E'(V_b)dU &(13)\\
&\geq -\int_{W_0}^{W_b} E'(V_b)dU + \int_{W_b}^{V_b} E'(U) - E'(V_b)dU \geq 0.
\end{aligned}$$

The inequality between (12) and (13) hold since an inequality holds between the first and second integrals of (12) and (13) respectively. The inequality between the first integral is obtained from the fact that for $U \in [W_0, V_\beta]$, $E'(U) \leq E'(V_b)$. For the inequality between the second integral we use $E'(V_b) > E'(V_T/2)$ and the fact that they each they represent the area of $E'(V)$ above the horizontal line of height $E'(V_T/2)$ and $E'(V_b)$ respectively.

□

Remark 1

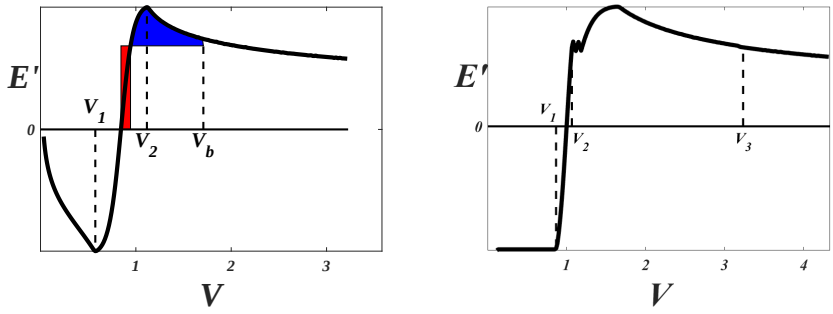

(a) $V - E'$ graph of hollow sphere (b) $V - E'$ graph of hollow cylinder

Fig. 8: Derivatives of the V-E graph for the hollow sphere and hollow cylinder (Fig. 5 and 6). In (a), V_b is chosen so that (11) is satisfied. The area in light red and dark blue represents the value of the left and right hand side of (11) respectively. The shape of the dropicle with water volume V_1 and V_2 are represented in Fig. 5a. In (b) the V_1, V_2 and V_3 are chosen to correspond to Theorem 4. The shape of the dropicle with water volume V_1 and V_2 are shown in Fig. 5 and 6 respectively. The unit volumes are V_{IS} and V_{IC} respectively. The surface tensions are $\sigma_{WO} = 1$, $\sigma_{WS} = 0.1$, $\sigma_{OS} = 0.9$.

1. The proof demonstrates a tighter bound $W_0 \leq V_S \leq W_b$ than $V_1 \leq V_S \leq V_2$. Note that W_0 is the minimum energy volume of the particle.
2. For the case of the V-E graph of a dropicle, as the volume increases the influence of the particle decreases and the energy of the dropicle asymptotes to that of a sphere. Therefore the second condition of the theorem

$$\lim_{V\to\infty} E'(V) \approx \lim_{V\to\infty} CV^{-1/3} = 0$$

   is justified.
3. For our purposes we deal with an excess amount of total volume, therefore V_b being small as possible is beneficial. We notice from the proof that V_b is small if $E'(V)$ increases rapidly between V_1 and V_2. This condition has another advantage that V_1 and V_2 are close to each other, which narrows the range in which V_S exists.

Application to the hollow sphere The derivative of the V-E graph of the hollow sphere is given in Fig. 8a. We have numerically calculated the values of V_1, V_2 and V_b. Theorem 3 predicts that when two hollow spheres are present the minimal surface energy configuration of a large volume of water is when one of the particles contains water of volume between V_1 and V_2 while the other contains the rest.

We can relax the conditions of Theorem 3 and get a similar result.

Theorem 4 *Let $E(V) \in \boldsymbol{C}^1[0,\infty)$ satisfy the same conditions as in Theorem 3 with a relaxation of condition 1 to*

1'. There exists $0 < V_1 < V_2 < V_3$ so that $E'(V)$ decreases for $0 \le V \le V_1$, increases for $V_1 \le V \le V_2$ and strictly decreases for $V_3 \le V$. Also $E'(V) > 0$ for all $V > V_2$.

Then for a total water of volume V_T the following are true,

1. *If $0 \le V_T \le V_1$, then $V_S = 0$ i.e. the minimal surface energy configuration is all water contained in one particle.*
2. *There exist a $V_b \ge V_3$ so that if $2V_b \le V_T$, then $V_1 \le V_S \le V_2$ i.e. there is a dropicle containing a drop in the volume range $[V_1, V_2]$.*

Proof. Fig. 8b is an example of a function that satisfies the conditions of the theorem. Most of the proofs are identical of that of Theorem 3. Only a modification of the proof is required for the second conclusion. In the second part of our proof the number of candidates do not change if we pick our total volume to be large enough that no volume in the range $[V_2, V_3]$ satisfies the (8). The comparisons between the candidates are identical except the comparison between $V_1 \le V_\beta \le V_2$ and $V = V_T/2$, which we present here.

Following the steps of the previous proof we want to show

$$\int_{V_\beta}^{V_T/2} E'(U) - E'(V_T/2)dU \ge 0.$$

For large enough V there is a unique W between V_1 and V_2 that $E'(W) = E'(V)$. Let W_0 be between V_1 and V_2 that satisfies $E'(W_0) = 0$. We pick a V_b so that the W_b corresponding to V_b satisfies

$$\int_{W_0}^{W_b} E'(V_b)dU \le \int_{W_b}^{V_b} E'(U) - E'(V_b)dU. \tag{14}$$

Such V_b exists since $\min_{V_2<V<V_3} E'(V) > 0$, and therefore for a large enough V_b increasing V_b results the left hand side of (14) going to 0 while the right hand side increases and stays positive. The rest of the proof is following the same steps of the previous proof. □

Application to the hollow cylinder Differentiating the V-E graph of the hollow cylinder (Fig. 8b) shows Theorem 4 is applicable. If there are two such particles and a large enough volume of water, the energy minimum is obtained when a volume between V_1 and V_2 is trapped in one of the particles.

3.2 Droplet splitting between many particles

In cases when we have more than two particles there is also a theorem about the minimum energy distribution. This is formulated as solving the optimization problem

$$\overline{W} = \underset{\Sigma W_i = W_T, W_i \geq 0}{\arg\min} \{\Sigma E(W_i)\}. \tag{15}$$

where $\overline{W}$ is a vector with N entries representing N particles and W_i being the water volume in i-th particle. The next theorem describes the water distribution on concave domains or convex domains of $E(V)$.

Theorem 5 *For an energy function $E(V)$ and $0 < a < b$, the minimization problem (15) has the following properties.*

1. *If $E(V)$ is concave in (a, b), then at most one of the entries of $\overline{W}$ is in (a, b).*
2. *If $E(V)$ is convex in $[a, b]$, then all the entries of $\overline{W}$ in the domain $[a, b]$ are equal.*

Proof. 1. Suppose not, i.e. there are two entries of the vector $\overline{W}$, W_i and W_j, that are between a and b. Then we can reduce the energy in (15) by increasing the difference between W_i and W_j, while keeping the total volume constant. By the definition of concave functions the energy decreases as we increase the difference between W_i and W_j to W_i' and W_j' (cf. (9)).

2. Suppose not, then there are two entries of $\overline{W}$, W_i and W_j, that are in $[a, b]$ and are different. Since $E(V)$ is convex in domain $[a, b]$, we can reduce the energy of the system by reducing the difference between the two entries. This is a contradiction, hence the entries with values in the domain $[a, b]$ are identical.

□

If $E(V)$ satisfies the conditions in Theorem 3, the value of the distribution $\overline{W}$ is proved rigorously, for sufficiently large total volume W_T.

Theorem 6 *Let $E(V)$ satisfy the conditions in Theorem 3 and let the total volume of water in the system W_T be larger than NV_b, then $N - 1$ entries of $\overline{W}$ are between V_1 and V_2.*

Proof. By Theorem 5 there are four possible values of the entries of $\overline{W}$: 0,V_l,V_m and V_u, where $0 < V_l < V_1 < V_m < V_2 < V_u$. We show that out of these values V_m and V_u are the only allowable ones. Notice by the total volume constraint there is an entry V_u, since otherwise all the entries of $\overline{W}$ are less then V_b which means that the total volume of water is less than NV_b. A second application of Theorem 5 shows us that there is only one entry with value V_u.

Suppose that entry i and j have water volume 0 and V_u respectively. Then $W_i + W_j = V_u > 2V_b$, by a total volume argument similar to above. Applying Theorem 3 to the two particle system with particle i and j, shows that the

distribution is not in the minimum energy state. Therefore $\overline{W}$ does not have any 0 entries. Similarly the case with an entry V_l is leads to a contradiction. □

The above theorem assures that in the lowest energy state, the particles have the same volume of water precisely when $E(V)$ is convex, except possibly one particle attached to a large volume, when the total volume is large enough (Section 5).

4 Numerical simulations of two particle splitting graphs

In this section we simulate pairwise interactions of a multi-particle system, in which fluid can be exchanged in a pairwise fashion to minimize the pairwise surface energy. The method randomly picks two particles, each with their own fluid volume, and redistributes the volume between the particles so as to minimize the surface energy of that two-particle system. This process is repeated until the ensemble reaches a steady state.

First we simulate the minimum energy distribution for two particles as a function of the total fluid volume. These simulations result in splitting graphs that show how the fluid is distributed. These results are consistent with the rigorous theory from the previous section. In [7], actual dynamic splitting experiments are done in the laboratory showing that the theoretical results are a reasonable approximation. However dynamic splitting is known to sometimes lead to local energy minima rather than the global minimizer.

4.1 Simulation of two particle system

First we consider the interaction of two identical particles. This corresponds to solving the optimization problem in section 3, which we restate here

$$V_S = \underset{0 \le V \le V_T/2}{\arg\min} \{E(V) + E(V_T - V)\}. \tag{16}$$

Once we specify $E(V)$, we can calculate $E(V) + E(V_T - V)$ for any given V_T and find V_S. We plot this optimal volume V_S as V_T varies, which we call the splitting graph. The splitting graphs of the hollow sphere and the hollow cylinder are given in Fig. 9.

Fig. 9a is the splitting graph of the hollow sphere (whose energy curve is plotted in Fig. 5a). The blue and red lines represent the volume of water in the two particles, while the dotted horizontal lines are the volumes V_1 and V_2 in Theorem 3. For small total volumes $V_S = 0$, while for large total volumes the smaller volume V_S is between V_1 and V_2. This agrees with Theorem 3. Note that the theorem does not provide a prediction in the intermediate range (domain that the droplets split evenly) which is straightforward to compute numerically.

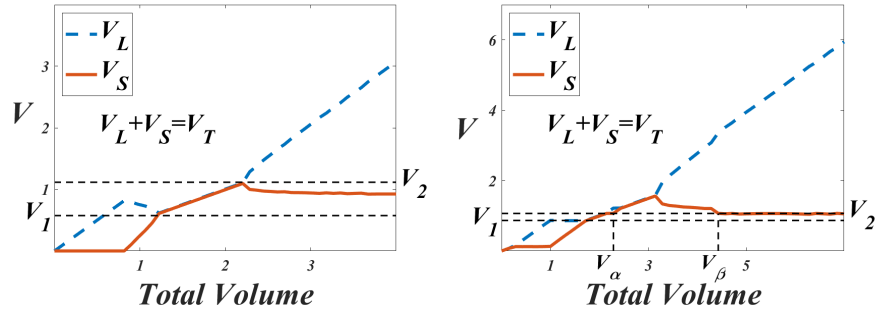

(a) Hollow sphere (b) Hollow cylinder

Fig. 9: Optimal splitting volume V_S of (16) with respect to V_T. (a) and (b) are the hollow spheres and hollow cylinders V-E graph respectively (Fig. 5a and 6a). V_L and V_S indicate the larger and smaller volume of the droplets ($V_L = V_T - V_S$), while the dotted horizontal lines V_1 and V_2 correspond to the volumes in theorems 3 and 4. The unit volumes are V_{IS} and V_{IC} respectively.

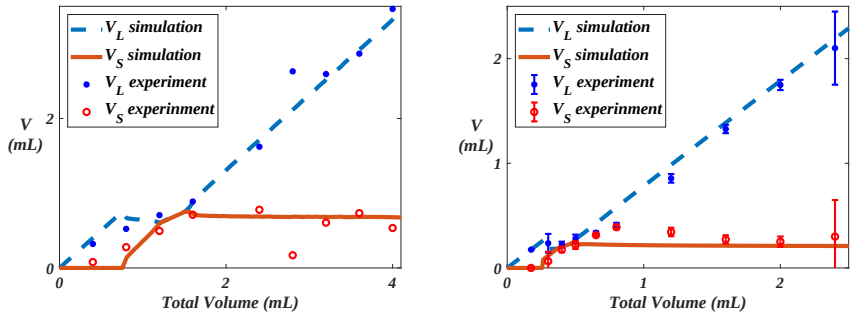

(a) Hollow sphere (b) Hollow cylinder

Fig. 10: Splitting graphs of the experiments and simulations [30]. The lines correspond to the simulations while the dots and bars correspond to the experiment data. The surface tensions for these graphs are matched to the materials in the experiments and therefore differ from the graphs in Fig. 9.

Fig. 9b is the splitting graph of the hollow cylinder (whose energy curve is plotted in Fig. 6a). Similar to the results of Fig. 9a the splitting graph agrees with Theorem 4.

The simulated splitting graph is compared to macroscale experiments [30]. The experiments use a hollow sphere and hollow cylinder particle about 10mm in diameter, with densities of the fluids closely matched. The particles are initially close together sharing the same aqueous volume. They are slowly pulled apart to minimize the effect of dynamics. To plot the splitting graph we need the surface tension of the particle. This is achieved by measuring

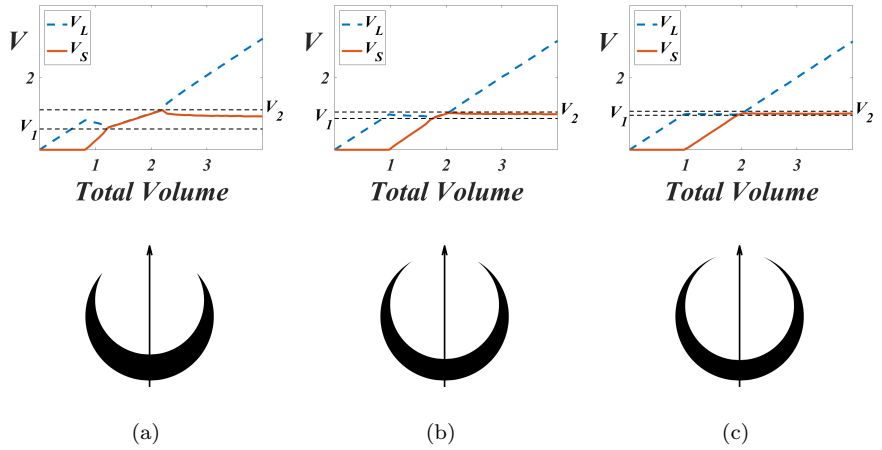

(a) (b) (c)

Fig. 11: Splitting graphs of various hollow sphere shapes. (a) is the particle that has a V-E graph of Fig. 5a. The shape is chosen so that r and R are fixed and d is 0.5, 0.8 and 0.9 for (a),(b) and (c) (parameters are in Fig. 3b). The unit volume is V_{IS} and the surface tensions are $\sigma_{WO} = 1$, $\sigma_{WS} = 0.1$, $\sigma_{OS} = 0.9$.

the contact angle and using (3). The results are shown in Fig. 10 which the theoretical splitting graph and the experiment results agree considerably.

In Fig. 9 we observe that the splitting graph of the cylindrical particle has a domain $[V_\alpha, V_\beta]$ where both particles contain water of volume greater than V_2. This is a disadvantage for our purposes, since we need a larger total volume than the spherical particle case to produce a water droplet of volume inside the range $[V_1, V_2]$. This indicates that the hollow sphere is a more promising particle geometry for achieving uniform droplets and as such we explore the spherical geometry for all subsequent simulations.

4.2 Different geometries and surface tensions

In this section we calculate the splitting graphs of the hollow sphere for different geometries and surface tensions. So far our computations are based on a specific shape of a hollow sphere and hollow cylinder with fixed surface tension values. In this case the splitting graph has two properties, (a) for small total volumes there is only one particle that contains water and (b) for large total volumes there is a volume range that one particle contains an amount of water volume within that range. We show that such results are robust in a sense that for a range of geometries and surface tensions the particles still possess these properties.

Fig. 11 shows the splitting graphs for spherical dropicles for three different geometries. The splitting graphs have the key features stated above. This

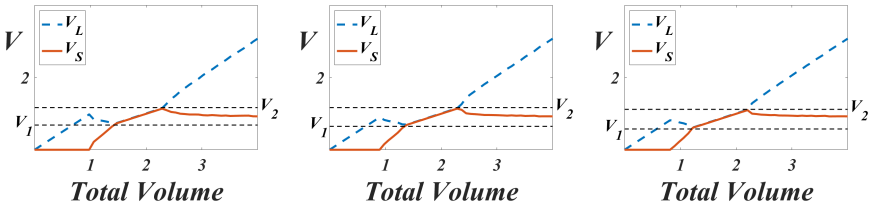

(a) σ_{OS}=0.5 (b) σ_{OS}=0.7 (c) σ_{OS}=0.9

Fig. 12: Splitting graphs of hollow spheres with different surface tensions. The shape of the particle is given in Fig.3b. Each graph has a different value of σ_{OS}, oil-solid surface tension. The surface tensions are 0.5, 0.7 and 0.9 for (a),(b) and (c) respectively. The other surface tensions are kept constant as $\sigma_{WS} = 0.1$ and $\sigma_{WO} = 1$. The unit volume is V_{IS}.

demonstrates that qualitative results are robust with respect to the geometry of the hollow sphere. We also observe a trend that the difference between V_1 and V_2 decreases as the opening of the particle becomes smaller. This suggests that it may be desirable to have a hollow sphere with a small opening to create more uniform volumes amongst a set of particles. However, practically if the opening is too small, it might be difficult for the fluid to exchange readily and the tip of the particle might be fragile and easy to break. Fig. 12 shows the splitting graphs as we change the surface tension between oil and solid, σ_{OS}, within the range of partial wetting. Such changes have almost no effect on the splitting graph, compared to the changes in the shape of the particle. This indicates that experiments are expected to behave similarly for a range of solid and fluid materials with different surface tensions.

5 Numerical simulations of multi-particle systems

For the multi-particle case we need to solve the optimization problem (15) which we restate here,

$$\overline{W} = \underset{\Sigma W_i = W_T, W_i \geq 0}{\arg\min} \{\Sigma E(W_i)\}. \tag{17}$$

If $E(V)$ satisfies the conditions of Theorems 3 and 4, together with Theorem 5, we predict that all except one of the nonzero entries of $\overline{W}$ have the same volume, as long as we start with sufficiently large total volume. Here we show numerically that this lowest energy state is achieved by repeated pairwise interactions. We consider a set of N dropicles that interact pairwise. The dropicles are chosen at random and fluid is exchanged between the pair to achieve the lowest energy state for that two particle system. The process is repeated with a different randomly chosen pair of particles. This randomized interaction is the simplest model to imitate the exchanging of fluid between

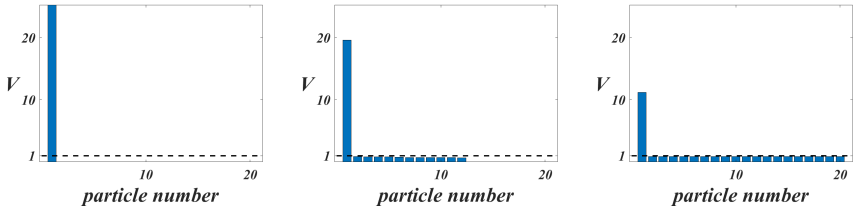

(a) Initial stage (b) Intermediate stage (c) Final stage

Fig. 13: The volume in each of the 20 spherical particles as they interact according to the randomized procedure. The initial condition is shown in (a) with all of the water in the first particle. (b) shows the result after $400 = 20^2$ iterations. (c) shows the end state after $4000 = 10 * 20^2$ iterations. In each figure the particle number is reordered in descending order. The unit volume is V_{IS}.

particles colliding at random during an agitation process leading to emulsification. For the geometries considered here, exclusively pairwise interactions are reasonable since not many dropicles can interact simultaneously with any other dropicle at a given time.

Randomized procedure

1. Initialize volume vector W, so that the sum of the entries is W_T. The initial state is a volume vector for N particles with all the water in the first particle.
2. Repeat the following until a fixed distribution of W_F is obtained.
   (a) Pick particles i and j at random and solve (15) for $V_T = W_i + W_j$.
   (b) Update $W_i = V_S$ and $W_j = V_T - V_S$.

Fig. 13 shows how the distribution changes as we increase the number of iterations. The volume that was initially attached to one particle distributes to other particles as they interact. Once the system reaches state Fig. 13c the minimum energy distribution is achieved (Theorem 6) and any additional interaction of the particles does not change the fixed distribution.

The fixed distributions W_F of a 100 particle system is shown in Fig. 14. The total volume of Fig. 14a and Fig. 14b are less than $100V_1$ and more than $100V_2$ respectively (V_1 and V_2 are those in Theorem 3). For the smaller total volume (Fig. 14a), the dropicles that are non empty have an identical amount of water. For the larger total volume (Fig. 14b), there is one dropicle that contains an excess amount of water while all the other dropicles have an identical amount. For both cases the identical amount of water is within the volume range of Theorem 3. Notice that in both cases most of the non-empty dropicles have a water volume between $[V_1, V_2]$, in agreement with Theorem 5 and 6. It is important to note that this volume range only depends on $E(V)$ and not the total volume of water.

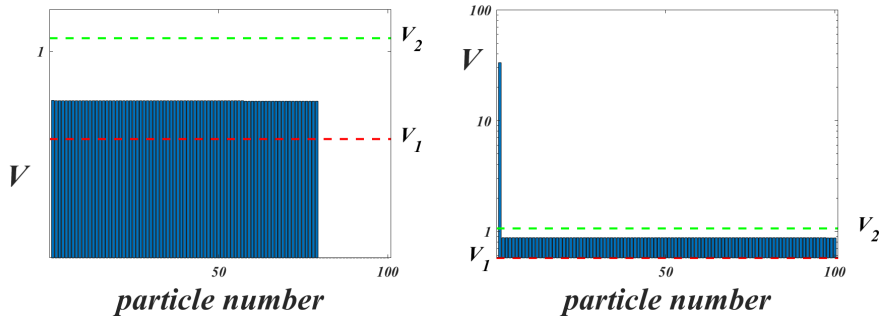

(a) (b)

Fig. 14: Fixed distribution of a 100 spherical particle systems. The total volume of (a) and (b) are 60 and 120 respectively. V_1 and V_2 are shown in red and green dotted horizontal lines. The y axis of (a) and (b) are in linear and logarithmic scale respectively. In each figure the particle number is reordered in descending order. The unit volume is V_{IS}.

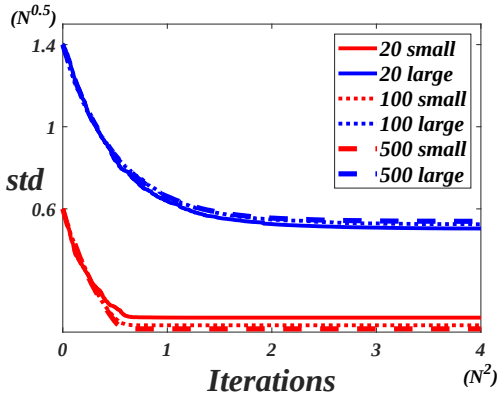

Fig. 15: Standard deviation of the volume vector W with respect to the number of iterations of pairwise interactions. Simulations are performed for systems with 20, 100, and 500 particles, each for two different total volumes. The red and blue lines correspond to the total volume of $0.6N$ and $1.4N$ respectively, where N is the number of particles. Each line shows the mean of 20 simulations. The number of iterations is normalized by N^2, and the standard deviation is normalized by $V_{IS}\sqrt{N}$, as the initial standard deviation scales with $\sqrt{N}$.

Another question is how many iterations are needed to achieve a final distribution. In physical experiments this corresponds to how much mixing is needed to distribute the water between all the particles. We numerically calculate the standard deviation of W as we increase the number pairwise of interactions (Fig. 15). We observe a decreasing trend and that it flattens out

once the system is fixed. Note that the number of iterations required is larger in the case of volume $0.6N$ compared to $1.4N$. This is due to the fact that the system with total volume $0.6N$ needs to fill less particles compared to the system with total volume $1.4N$. Also notice that the curves with different numbers of particles overlap for total volume $0.6N$ and $1.4N$. This indicates that there is a general trend that determines the number of interactions.

6 Conclusion

This paper develops a fundamental theory for the distribution of fluid between microscale "dropicles" in the case of axisymmetry. Previous work on the minimal energy state of multi phase fluid-solid interactions was limited to the classic problem of a catenoidal liquid bridges [28]. This work develops the necessary theory for modern "dropicle" interactions that are of particular interest in emerging "lab on a particle" technologies [7,9]. Using the generated minimal energy volume curves, we predict that randomized pairwise interactions between multiple dropicles has a long-time equilibrium distribution with effectively uniform water volumes adhering to each particle, except for a sole dropicle with excess volume.

As we have explored in section 4.2, as long as the shape and surface tension of the particles are within the range of physical interest, we get a water droplet of size within the range $[V_1, V_2]$, as specified in Theorem 3 and 4. Here we consider minimizing the interval size $[V_1, V_2]$ to better uniformize the water droplet size. Likewise minimizing V_b in Theorem 3 and 4 reduces the size of the excess volume needed to guarantee this distribution. Further work could (a) define a quantitative measure that estimates the effectiveness of a particle to achieve high droplet uniformity and reduction of the required excess total volume and (b) optimize the particle to maximize this measure.

Another question is to understand the number of iterations needed to obtain the final distribution. This is related to the degree of physical mixing required to achieve a good distribution in practice. We propose the standard deviation of the volume vector W (Fig. 15) as a way of determining if W is a fixed distribution. However this method requires expensive computations. Instead we would like a inexpensive method of calculating the required number of iterations.

Comparing our simulations to the experimental data we find that they agree to a large extent (Fig. 10). However there are assumptions in our model that contribute to the discrepancy between simulations and physical experiments. For example, two particle experiments may achieve a local energy minimum rather than a global one, including the possibility of the formation of satellite drops as shown in experiments on capillary breakup [31].

Theorem 1 enables us to explore other axisymmetric particles other than hollow spheres and cylinders. However many axisymmetric shapes are difficult to manufacture at the microscale. An alternative non-axisymmetric shape is

considered in [7] and the V-E energy graph argument is used, albeit with much more computationally expensive fully 3D simulations for the energy.

Acknowledgement

This work is supported by the Simons Math + X project (510776). Fig. 10 was generated by an REU team during the summer of 2019 supported by the NSF (DMS-1659676). The team members include Bernardo Hernandez Adame, Ryan Shijie Du, Lily Liu, Simon Ng, Hansell Perez, Sneha Sambandam, Claudia Falcon.

References

1. Takahiro Kawakatsu, Yuji Kikuchi, and Mitsutoshi Nakajima. Regular-sized cell creation in microchannel emulsification by visual microprocessing method. *Journal of the American Oil Chemists' Society*, 74(3):317–321, 1997.
2. Shelley L Anna, Nathalie Bontoux, and Howard A Stone. Formation of dispersions using flow focusing in microchannels. *Applied physics letters*, 82(3):364–366, 2003.
3. Yung-Chieh Tan, Vittorio Cristini, and Abraham P Lee. Monodispersed microfluidic droplet generation by shear focusing microfluidic device. *Sensors and Actuators B: Chemical*, 114(1):350–356, 2006.
4. Hsiang-Wei Lu, Frederic Bottausci, Jesse D Fowler, Andrea L Bertozzi, Carl Meinhart, et al. A study of ewod-driven droplets by piv investigation. *Lab on a Chip*, 8(3):456–461, 2008.
5. Wyatt C Nelson and Chang-Jin CJ Kim. Droplet actuation by electrowetting-on-dielectric (ewod): A review. *Journal of Adhesion Science and Technology*, 26(12-17):1747–1771, 2012.
6. Heng-Dong Xi, Hao Zheng, Wei Guo, Alfonso M Gañán-Calvo, Ye Ai, Chia-Wen Tsao, Jun Zhou, Weihua Li, Yanyi Huang, Nam-Trung Nguyen, et al. Active droplet sorting in microfluidics: a review. *Lab on a Chip*, 17(5):751–771, 2017.
7. Chueh-Yu Wu, Bao Wang, Joseph de Rutte, Mengxing Ouyang, Alexis Joo, Matthew Jacobs, Kyung Ha, Andrea L. Bertozzi, and Dino Di Carlo. Monodisperse drops templated by 3d-structured microparticles. *Nature communications, accepted*.
8. Ghulam Destgeer, Mengxing Ouyang, Chueh-Yu Wu, and Dino Di Carlo. Fabrication of 3d concentric amphiphilic microparticles to form uniform nanoliter reaction volumes for amplified affinity assays. *Lab on a Chip*, 2020.
9. Joseph de Rutte, Robert Dimatteo, Mark van Zee, Robert Damoiseaux, and Dino Di Carlo. Massively parallel encapsulation of single cells with structured microparticles and secretion-based flow sorting. *bioRxiv*, 2020.
10. Andrew J Bernoff, Andrea L Bertozzi, and Thomas P Witelski. Axisymmetric surface diffusion: dynamics and stability of self-similar pinchoff. *Journal of statistical physics*, 93(3-4):725–776, 1998.
11. JB Bostwick and PH Steen. Stability of constrained capillary surfaces. *Annual Review of Fluid Mechanics*, 47, 2015.
12. G Mason and WC Clark. Liquid bridges between spheres. *Chemical Engineering Science*, 20(10):859–866, 1965.
13. Olivier Pitois, Pascal Moucheront, and Xavier Chateau. Liquid bridge between two moving spheres: an experimental study of viscosity effects. *Journal of colloid and interface science*, 231(1):26–31, 2000.
14. Yakov I Rabinovich, Madhavan S Esayanur, and Brij M Moudgil. Capillary forces between two spheres with a fixed volume liquid bridge: theory and experiment. *Langmuir*, 21(24):10992–10997, 2005.

15. Lev A Slobozhanin, J Iwan D Alexander, and Viral D Patel. The stability margin for stable weightless liquid bridges. *Physics of Fluids*, 14(1):209–224, 2002.
16. Dieter Strube. Stability of a spherical and a catenoidal liquid bridge between two parallel plates in the absence of gravity. In *Microgravity Fluid Mechanics*, pages 263–269. Springer, 1992.
17. Thomas I Vogel. Stability of a liquid drop trapped between two parallel planes. *SIAM Journal on Applied Mathematics*, 47(3):516–525, 1987.
18. Thomas I Vogel. Stability of a liquid drop trapped between two parallel planes ii: General contact angles. *SIAM Journal on Applied Mathematics*, 49(4):1009–1028, 1989.
19. Lianmin Zhou. On stability of a catenoidal liquid bridge. *pacific journal of mathematics*, 178(1):185–198, 1997.
20. Michael A Erle, RD Gillette, and DC Dyson. Stability of interfaces of revolution with constant surface tension-the case of the catenoid. *The Chemical Engineering Journal*, 1(2):97–109, 1970.
21. RD Gillette and DC Dyson. Stability of fluid interfaces of revolution between equal solid circular plates. *The Chemical Engineering Journal*, 2(1):44–54, 1971.
22. Lev A Slobozhanin, Valentina M Shevtsova, J Iwan D Alexander, José Meseguer, and José M Montanero. Stability of liquid bridges between coaxial equidimensional disks to axisymmetric finite perturbations: a review. *Microgravity Science and Technology*, 24(2):65–77, 2012.
23. Matthew J Russo and Paul H Steen. Instability of rotund capillary bridges to general disturbances: experiment and theory. *Journal of colloid and interface science*, 113(1):154–163, 1986.
24. Brian J Lowry and Paul H Steen. Stability of slender liquid bridges subjected to axial flows. *Journal of Fluid Mechanics*, 330:189–213, 1997.
25. Brian James Lowry and Paul H Steen. Capillary surfaces: stability from families of equilibria with application to the liquid bridge. *Proc. R. Soc. Lond. A*, 449(1937):411–439, 1995.
26. RD Gillette and DC Dyson. Stability of axisymmetric liquid-fluid interfaces towards general disturbances. *The Chemical Engineering Journal*, 3:196–199, 1972.
27. Lev A Slobozhanin and José M Perales. Stability of an isorotating liquid bridge between equal disks under zero-gravity conditions. *Physics of Fluids*, 8(9):2307–2318, 1996.
28. Amir Akbari, Reghan J Hill, and Theo GM van de Ven. Catenoid stability with a free contact line. *SIAM Journal on Applied Mathematics*, 75(5):2110–2127, 2015.
29. Anatolii D Myshkis, Vitalii G Babskii, Nikolai D Kopachevskii, Lev A Slobozhanin, Anatolii D Tyuptsov, and RS Wadhwa. Low-gravity fluid mechanics. *Translated from the Russian by Wadhwa, RS, XIX, 583 pp. 218 figs.. Springer-Verlag Berlin Heidelberg New York*, page 218, 1987.
30. Ryan Shijie Du, Lily Liu, Simon Ng, Sneha Sambandam, Bernardo Hernandez Adame, Hansell Perez, Kyung Ha, Claudia Falcon, Joseph de Rutte, Dino Di Carlo, and Andrea L. Bertozzi. Statistical energy minimization theory for systems of drop-carrier particles. *In preparation*.
31. Mahari Tjahjadi, Howard A Stone, and Julio M Ottino. Satellite and subsatellite formation in capillary breakup. *Journal of Fluid Mechanics*, 243:297–317, 1992.